electronics

MDPI

Article

An Anti-Interference Method Based on Energy Residual Searching in GNSS Positioning Applications

Xiaobing Jiang [1], Ming Lei [1], Yimeng Niu [2], Jiashan Wan [2] and Na Xia [2,*]

[1] State Grid Electric Power Research Institute Co., Ltd., Nanjing 210000, China; jiangxiaobing@sgepri.sgcc.com.cn (X.J.); leiming@sgepri.sgcc.com.cn (M.L.)
[2] School of Computer Science and Information Engineering, Hefei University of Technology, Hefei 230601, China; 2023110469@mail.hfut.edu.cn (Y.N.); jswanwo@gmail.com (J.W.)
* Correspondence: xiananawo@hfut.edu.cn

Abstract: Addressing the issue of linear frequency modulation (LFM) interference in GNSS positioning, this paper proposes an interference suppression method based on energy residual searching, incorporating the fractional Fourier transform (FrFT) for improved performance. In GNSS systems, LFM interference can severely impair positioning accuracy and system robustness, potentially rendering the receiver incapable of performing accurate localization. To address this issue, an energy residual function is introduced to quantitatively assess the impact of interference on the original signal. This function combines differences in signal energy with signal quality after spectral line removal to achieve effective interference evaluation. By optimizing the parameters of the fractional Fourier transform to maximize the value of the energy residual function the proposed method significantly enhances interference suppression. Our experimental results demonstrate that the method performs exceptionally well on practical datasets, effectively removing interference and restoring relevant peaks. This approach mitigates the negative effects of LFM interference on GNSS positioning performance, substantially improving both positioning accuracy and system robustness.

Keywords: global navigation satellite system; interference detection and mitigation; fractional Fourier transform; signal acquisition

check for updates

Citation: Jiang, X.; Lei, M.; Niu, Y.; Wan, J.; Xia, N. An Anti-Interference Method Based on Energy Residual Searching in GNSS Positioning Applications. *Electronics* **2024**, *13*, 4713. https://doi.org/10.3390/electronics13234713

Academic Editor: Valeri Mladenov

Received: 10 October 2024
Revised: 2 November 2024
Accepted: 11 November 2024
Published: 28 November 2024

Correction Statement: This article has been republished with a minor change. The change does not affect the scientific content of the article and further details are available within the backmatter of the website version of this article.

Copyright: © 2024 by the authors. Licensee MDPI, Basel, Switzerland. This article is an open access article distributed under the terms and conditions of the Creative Commons Attribution (CC BY) license (https://creativecommons.org/licenses/by/4.0/).

1. Introduction

With the increasing number of applications utilizing global navigation satellite systems (GNSS), demand for reliable navigation and timing has significantly increased, encompassing critical fields such as transportation, energy systems, telecommunications, and emergency response. Previously, GNSS were predominantly employed for static geodetic measurements. However, their functionality has evolved to include dynamic measurements across various domains, such as land, marine (hydrographic), and aerial navigation. This transition highlights the expanding role of GNSS in meeting the diverse demands of modern navigation and positioning needs.

The GNSS signals used in most satellite navigation systems [1] are typically designed with a direct-sequence spread spectrum (DSSS) scheme, which provides inherent resistance to electromagnetic interference. However, due to the significant distance between navigation satellites and receivers, the received GNSS signal strength is usually very weak by the time it reaches Earth. This low signal strength makes GNSS signals highly susceptible to interference from complex electromagnetic environments [1–3], as illustrated in Figure 1, especially around power facilities. Sources of such interference include, but are not limited to, power line harmonics, switching electromagnetic interference, and electromagnetic radiation from the power equipment itself. These interference sources can degrade GNSS signal quality, potentially causing errors in positioning and timing calculations, which, in turn, can impact the safety and reliability of power systems. Therefore, the development and the application of effective anti-interference algorithms to enhance GNSS signal reception and

processing in power scenarios are crucial for ensuring the safe operation of power facilities and improving the management efficiency of energy systems.

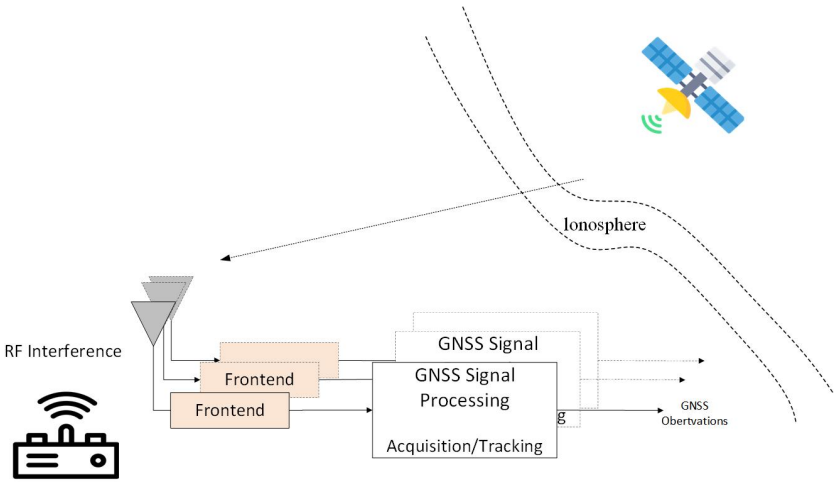


Figure 1. GNSS receivers are susceptible to RF interference.

Among the various types of interference, linear frequency modulation (LFM) interference [3–5] is a common and typical form of broadband non-stationary interference widely employed to disrupt navigation signals. Compared to other types of interference, LFM interference has several notable characteristics [4]: firstly, the equipment required to generate this type of interference is relatively simple and low-cost, making it a frequently used method of interference; secondly, the frequency of LFM interference varies linearly with time, endowing it with powerful interference capabilities, which makes it difficult for conventional GNSS receivers to detect and suppress. This threat is particularly pronounced in power-related environments, where the electromagnetic conditions are complex and variable, exacerbating the impact of LFM interference on GNSS signals. It should be noted that while this study primarily focuses on anti-LFM interference in power environments, the proposed anti-interference method is versatile and can be applied beyond power scenarios. Countermeasures against LFM interference include techniques such as adaptive notch filtering [6–9], time–frequency analysis [10], and array antenna methods [11,12]. Time–frequency analysis, in particular, is widely applied, due to its ability to process signals simultaneously in the time and frequency domains, capturing the non-stationary characteristics of the interference signal. Compared with other methods, time–frequency analysis provides more detailed information on the interference, aiding in the precise localization and identification of interfering signals. Commonly used time–frequency analysis techniques include short-time Fourier transform (STFT), wavelet transform, and the Wigner–Ville distribution, all of which have been extensively employed for detecting and mitigating LFM interference.

However, traditional time–frequency analysis techniques also have certain limitations. STFT, for example, cannot simultaneously achieve high time and frequency resolution, due to its fixed window size. Wavelet transform, while partially addressing this issue, suffers from high computational complexity and limited real-time capabilities. The Wigner–Ville distribution, on the other hand, has cross-term interference issues, complicating signal analysis. To overcome these limitations, this paper proposes an anti-interference method based on the fractional Fourier transform (FrFT). The FrFT provides flexible resolution capabilities, allowing it to better adapt to the characteristics of LFM interference and achieve effective suppression of the interfering signal. In this study, we innovatively propose an energy residual search method, which enhances interference detection and suppression on the basis of the FrFT, ensuring reliable GNSS receiver performance in complex electromagnetic environments. The subsequent chapters of this paper are organized as follows: Section 2 presents a review of related work; Section 3 discusses the GNSS received signal model;

Section 4 describes the energy residual search-based anti-interference method; Section 5 presents the experimental results, including a comparison of detection performance among various algorithms; and Section 6 concludes the paper.

2. Related Work

When discussing the relevant work on counteracting GNSS interference, time–frequency domain analysis techniques emerge as particularly significant. Linear frequency modulation (LFM) wideband or continuous-wave narrowband interference signals can generate highly concentrated energy distributions on the time–frequency (TF) plane. The short-time Fourier transform (STFT) decomposes a long signal into multiple short segments, performing Fourier transforms on each segment, thereby providing simultaneous information about both the time and frequency of the signal. Consequently, many researchers [13–16] have developed a series of interference suppression algorithms based on STFT and its variants. For instance, Xuemei Ouyang [13] proposed an adaptive interference cancellation technique based on STFT, effectively mitigating non-stationary and rapidly varying interference in direct sequence/spread spectrum (DS/SS) communication systems. Wang Pai [14] introduced an interference detection method utilizing time–frequency statistical analysis based on STFT, discussing the impact of traditional STFT and block STFT techniques on detection effectiveness. However, the application of STFT for interference detection and mitigation still faces several limitations. Firstly, STFT suffers from an inherent trade-off between time and frequency resolution, making it challenging to achieve high resolution in both domains simultaneously [16,17]. Additionally, the computational complexity of STFT presents challenges for real-time processing of long time series or high-sampling-rate signals.

To circumvent the trade-off issue in time–frequency resolution, many scholars have employed the Wigner–Ville distribution (WVD) for detecting linear frequency-modulation interference. The WVD offers many advantageous properties, providing nearly the best resolution among all time–frequency distributions. However, due to the interaction of different components, it exhibits significant cross terms in the time–frequency plane, leading to considerable errors in the instantaneous frequency estimation of interference signals. Techniques such as smoothing can be utilized to mitigate the impact of these cross terms. KeWen Sun proposed a novel frequency-sweep interference detection and suppression method based on the Radon–Wigner transform (RWT), which effectively alleviates the cross-term issues prevalent in traditional time–frequency analysis techniques. Pai Wang [18] introduced a pseudo Wigner–Ville distribution that effectively addresses both narrowband and wideband interference while possessing a degree of cross-term suppression capability. Leon [19] proposed a pseudo Wigner–Ville distribution (PWVD) that partially suppresses cross terms by employing window functions in the time domain, although this approach can lead to a decrease in resolution. Auger [20] introduced a smoothed pseudo Wigner–Ville distribution (SPWVD), which allows for independent and progressive control in both the time and frequency directions, offering flexibility in alleviating poor cross-term conditions in the WVD. While this method can suppress interference terms, it requires careful parameter tuning, resulting in a relatively complex implementation. KeWen Sun [21] proposed a new joint hybrid time–frequency analysis method based on the Choi–Williams transform, the Hadamard product, and the smoothed pseudo-Wigner–Ville distribution, effectively eliminating cross terms present in bilinear TF distributions. In addition, he also proposed several variants of the Wigner distribution [22–24].Furthermore, combining the Wigner transform with the Hough transform has facilitated the development of GNSS interference detection techniques based on the Wigner–Hough transform [23,25,26]. For example, in [25] a GNSS interference detection method based on the smoothed pseudo-multi-resolution Hough transform was proposed, to improve detection performance by addressing the cross-term issue, transforming GNSS interference detection into a localized search for Hough transform energy peaks within a small region of the polar Hough parameter space.

In comparison to traditional time–frequency analysis methods, the fractional Fourier transform (FrFT) [27,28] has garnered significant attention, due to its effectiveness in handling the characteristics of signals such as LFM. The FrFT avoids the introduction of cross-interference terms, thereby better preserving the original time–frequency characteristics of the signal. Additionally, linear frequency-modulation interference can exhibit good energy concentration in the optimal fractional Fourier domain, while useful GNSS signals and additive white Gaussian noise (AWGN) are typically dispersed throughout the fractional Fourier domain without any energy concentration [29,30]. This characteristic highlights the theoretical and practical significance of FrFT in GNSS receiver applications. Once the optimal fractional order of the FrFT is determined, effective detection of GNSS frequency-sweep interference signals can be achieved by searching for energy peaks within the fractional Fourier domain.

3. Signal Model

The signal transmitted by the satellite includes navigation messages, PRN codes, and a carrier wave. The signals from different pseudorandom noise (PRN) codes are superimposed, to form the signal received by the receiver. LFM interference spreads across the entire spectrum and masks the true signal, thereby degrading the receiver's performance. The receiver utilizes the signal received by the antenna, which is mixed to an intermediate frequency (IF) through the RF front end. At this stage, the IF signal consists of the true signal, LFM interference, and noise, and it can be expressed as follows:

$$\begin{aligned} r(nT_s) = &\sum_{i\in\alpha} A_i C_i(nT_s-\tau_i) D_i(nT_s-\tau_i) e^{j2\pi(f_{IF}+f_i)nT_s+j\phi} \\ &+ j_R F(nT_s) + N(nT_s) \end{aligned} \tag{1}$$

where A, C, and D represent the amplitude of the satellite signal, the PRN code, and the navigation message, respectively; $e^{j(\cdot)}$ represents the complex carrier, with its real and imaginary parts corresponding to the in-phase and quadrature components of the signal; n denotes the discrete-time variable; τ_i, f_{IF}, f_i, and ϕ correspond to the code phase delay, intermediate frequency, carrier frequency, and initial signal phase, respectively; α represents the set of all satellite signals, and the subscript i denotes the i-th satellite in the satellite set; N denotes Gaussian white noise with a mean of zero; and $j_{RF}(nT_s)$ represents the non-stationary GNSS LFM interference signal generated by the jammer, which can be expressed as

$$j_{RF}(nT_s) = A_j cos[2\pi(f_0 nT_s + \frac{1}{2}kn^2T^2 + \phi_j]e^{j2\pi(f_{IF}+f_i)nT_s+j\phi} \tag{2}$$

where A_j denotes the amplitude of the LFM interference signal; f_0 denotes the initial frequency; k denotes the frequency sweep rate; ϕ_0 denotes the initial phase of the LFM signal; T_s denotes the the sampling period; f_{IF} denotes the intermediate frequency; f_i denotes the carrier frequency; and ϕ denotes the initial signal phase.

4. Anti-Interference Method Based on Energy Residual Searching

4.1. Constructing the Energy Residual Function

First, a predefined FrFT is applied to the digitized downconverted analytic signal using a preset fractional order (although this order may not be the optimal one). This step aims to concentrate the energy of the LFM interference signal in the transform domain, without causing the energy of the noise and GNSS signals to concentrate. The fractional Fourier transform of the analytic signal can be expressed as

$$F^p[x](\frac{m}{2\triangle x}) = \frac{A_a}{2\triangle x} exp[j\pi(\gamma-\beta)(\frac{m}{2\triangle x})^2]\cdot \sum_{n=-(\triangle x)^2}^{(\triangle x)^2} exp[j\pi\beta(\frac{m-n}{2\triangle x})^2] exp[j\pi(\gamma-\beta)(\frac{m}{2\triangle x})^2] x(\frac{n}{2\triangle x}) \tag{3}$$

where F represents the Fourier transform operator; p denotes the fractional order of the Fourier transform; j is the imaginary unit; A_a denotes the transformation coefficient; α is the transformation angle; $\beta = csc\alpha$; $\gamma = cot\alpha$; m denotes a discrete sampling point variable in the transformation domain; $\triangle x = \sqrt{T_{obs}/T_s}$ denotes the normalized width; and T_{obs} denotes the time duration of the processed signal. For simplicity, we denote $F^p[x](\frac{m}{\triangle x})$ as $x_p[\frac{m}{\triangle x}]$.

The summation part in the above equation is a discrete convolution, which can be computed using FFT, with a complexity of $NlogN$.

To determine the threshold value for spectral line excision, the N-sigma method is an appropriate choice. The rationale behind this is that when the LFM signal is transformed into a pulse function in the fractional domain, its energy is concentrated on a few spectral lines, while the remaining data points exhibit relatively low values and a more uniform distribution. The N-sigma method effectively identifies these significant spectral lines, thereby enabling the determination of a reasonable threshold value. Specifically, the threshold can be expressed as

$$Th = K * \delta + \mu \tag{4}$$

where μ represents the mean value of the spectral line amplitudes; δ denotes the standard deviation of the spectral line amplitudes; and K denotes the selected multiplication factor used to control the stringency of identifying outlier spectral lines. After calculating the threshold value, spectral components in the transform domain with amplitudes exceeding this threshold are excised. This step effectively suppresses the high-amplitude components of the signal in the transform domain. Specifically, the process of spectral line excision can be represented as

$$x_p[\frac{m}{\triangle x}] = \begin{cases} 0, & x_p[\frac{m}{\triangle x}] > Th \\ x_p[\frac{m}{\triangle x}], & x_p[\frac{m}{\triangle x}] \leq Th \end{cases} \tag{5}$$

Based on the computed threshold value, spectral components with amplitudes exceeding this threshold are removed. The energy of the transformed-domain signal is then calculated after the spectral line removal:

$$E_1 = \sum_{n=-(\triangle x)^2/2}^{(\triangle x)^2/2} |x[\frac{n}{\triangle x}]|^2 \tag{6}$$

We calculate the signal energy in the transformed domain before the spectral line removal. According to Parseval's theorem, the energy of the transformed-domain signal before removal is equal to the energy of the analytic signal:

$$E_2(p) = \sum_{m=-(\triangle x)^2/2}^{(\triangle x)^2/2} [|x_p|\frac{m}{\triangle x}|^2] \tag{7}$$

Based on the aforementioned, the energy residual function is constructed. The energy residual refers to the reduction in signal energy after the spectral line removal, reflecting the extent to which high-amplitude components have been removed. Specifically, it can be expressed as

$$res(p) = |E_1 - E_2(p)^2| \tag{8}$$

The significance of the energy residual lies in its ability to quantitatively assess the suppression effect of the LFM interference signal in the transform domain. A larger energy residual indicates that more LFM interference signal components have been effectively removed in the transform domain, while a smaller energy residual suggests that fewer interference components have been removed. By optimizing the fractional order parameters to maximize the energy residual, the optimal fractional Fourier transform can be identified, achieving the maximum suppression of LFM interference signal energy in the transform domain and, thereby, enhancing the GNSS signal's interference resistance. Specifically, the optimal fractional order can be expressed as

$$\arg \max_{p\in[0,2]} |E_1 - E_2(p)^2| \tag{9}$$

The energy residual function transforms multi-peaked, multi-periodic spectral lines into a one-dimensional single-extreme function, altering the structure of the interference suppression algorithm. This modification reduces the search dimensions and significantly enhances the efficiency of solving for the optimal transform order.

4.2. Performing Peak Searching on the Energy Residual

The non-interpolative root mean square method is employed to perform peak searching on the one-dimensional energy residual function. Initially, the step size, error tolerance, and starting point are specified. Subsequently, search sequences are determined, using Equations (10) and (11), and an initial search interval is constructed:

$$\begin{cases} u_0 = a \\ g(u_0) = -res(u_0) \end{cases} \tag{10}$$

$$\begin{cases} u_i = F_i \cdot T_0 + a, & i = 1, 2, 3, ..., n \\ g(u_i) = -res(u_0), & g(u_{n-1}) < g(u_0), g(u_n) > g(u_0) \end{cases} \tag{11}$$

where F_n denotes the n-th Fibonacci number; u_i denotes the i-th search variable (with a maximum value not exceeding 2); g_i denotes the i-th search function (obtained by inverting the energy residual function calculated in the previous steps); and n is the number of search points. The initial point u_0 of the search interval is set to the starting point a_0, and the end point of the search interval is determined as the first search variable where the value of the search function exceeds that of the initial search function. If $n < 2$, the initial step size is reduced to one third of its original value and the above steps are repeated until a reasonable search sequence and search interval are obtained.

The root mean square values of the aforementioned points are computed using Equation (12), and these values are inserted into the search sequence in ascending order of the search variables. We let the point that minimizes the energy residual function within the search interval be denoted as B, with its left neighboring point as A and its right neighboring point as C. A new search sequence and interval are constructed based on these three points, and the root mean square values of these three points are calculated using Equation (13):

$$u_{rms,k} = \sqrt{\frac{\sum_{i=0}^{n} u_i^2}{n+1}}, k = 0 \tag{12}$$

$$u_{rms,k} = \sqrt{\frac{A^2 + B^2 + C^2}{3}}, k = k + 1 \tag{13}$$

Based on the calculated mean square values, we assume ε is the noise tolerance, if the condition $|u_{rms,k} - u_{rms,k-1}| < \varepsilon |u_{rms,k}|$ is met, the iteration is terminated, and the mean square value point is selected as the peak of the energy residual function. Otherwise, the calculated mean square value point is added to the search sequence, a new search

interval is constructed according to Equation (11), and the mean square value is recalculated as per Equation (13). The process then returns to this step.

Using the peak points of the energy residual function obtained from the search, we perform the fractional Fourier transform (FRFT) inverse transformation according to the order specified in (3). This process yields the discrete GNSS satellite original signal after the interference has been filtered out.

Based on the above analysis, the procedure of the proposed non-interpolative root mean square method is shown in Algorithm 1.The overall algorithm structure is shown in Algorithm 2. The overall computational complexity of our method is as follows: the FrFT has a complexity of $O(NlogN)$, the optimization process employs a variant of the Fibonacci search with a complexity of $O(logN)$, and the energy residual calculation has a linear complexity of $O(N)$. Given these complexity levels, the combined approach can be efficiently executed on platforms with moderate computational capabilities, ensuring feasibility for applications that require real-time or near-real-time processing.

Algorithm 1 Peak Searching with Non-Interpolative Root Mean Square Method

Notations:
$U = [u_0, u_1, \ldots, u_n]$: The search point sequence.
$G = [g(u_0), g(u_1), \ldots, g(u_n)]$: The objective function sequence.
$u_{\mathrm{rms},k}$:The root mean square value.
ε :The error tolerance.
T_0 :The initial step size
ε :The error tolerance
a :The starting point
p :Optional fractional order

Input: T_0, ε, a.
Output: p.
Step 1: Compute the search sequence U and the objective function sequence G by (12) and (13).
Step 2: Compute the RMS value $u_{\mathrm{rms},k}$ of the search points by (14), and insert it into U in ascending order of the search points.
Step 3: Identify the minimum point B and its neighboring points by (15).
Step 4: Update the RMS value $u_{\mathrm{rms},k}$ of the search point sequence by (16).
Step 5: If $|u_{rms,k} - u_{rms,k-1}| < \varepsilon |u_{rms,k}|$ is satisfied ,Terminate the iteration and select the current RMS value $u_{rms,k}$ as the peak point p;
Step 6: Else,Construct a new search point sequence according to (11) and to **Step 2**

Algorithm 2 The overall algorithm structure

Input: Intermediate frequency (IF) signal containing interference, initial fractional order.
Output: Filtered IF signal.
Step 1: Apply the FrFT to the signal using Equation (3).
Step 2: Compute the energy residual using Equation (8).
Step 3: Perform energy residual search using Algorithm 1 to determine the optimal fractional order p^*.
Step 4: Determine the threshold using Equation (4) and apply spectral line removal using Equation (5).
Step 5: Apply the inverse fractional Fourier transform using Equation (3) to obtain the filtered signal.

5. Simulation and Results

The experiments were conducted in a high-performance computing environment, to ensure efficient execution of the complex algorithms and data processing tasks. The hard-

ware configuration included an Intel Core i7-12700K CPU with 12 cores and 20 threads, operating at a base clock of 3.6 GHz and capable of reaching a maximum turbo frequency of 5.0 GHz. The system was equipped with 16 GB of DDR4 RAM, operating at 3200 MHz, providing sufficient memory for large-scale data processing and memory-intensive computations. Additionally, an NVIDIA GeForce RTX 2070 GPU with 8 GB of GDDR6 memory was utilized to accelerate the image processing and deep learning model training. The software environment for this study was MATLAB 2023b, which was employed for its robust mathematical computation and simulation capabilities, along with various toolboxes for data processing, algorithm development, and simulation. This setup provided the necessary computational resources to ensure the reliability and accuracy of the experiment's results.

To validate the effectiveness and feasibility of the proposed interference detection method based on the fractional Fourier transform (FrFT), multiple tests were conducted, with the relevant parameters listed in Table 1. The intermediate frequency (f_{IF}) of the GNSS software receiver((FGI-GSRx v2.0.1)) was set to 40.42 MHz, and the sampling frequency (f_s) was set to 25 MHz, in accordance with the bandpass sampling theorem. The collected GPS L1-C/A signals were disturbed by constant-amplitude linear frequency modulation (LFM) interference (i.e., linear chirp) in zero-mean white noise, which is commonly used as an interference detection test platform in GNSS applications. In the GNSS interference detection tests, the jamming-to-noise ratio (JNR) of the linear chirp was set to -4 dB, the sweep period was set to 0.5 ms, and the chirp rate was set to 25 GHz/s.

Table 1. Experimental parameters in interference detection test.

Parameter	Value
Carrier-to-noise ratio, C/N_0	46 dB-Hz
Jammer-to-noise ratio, JNR	-4 dB
Sampling frequency	25 MHz
Intermediate frequency	40.42 MHz
Frequency rate of change	25 GHz/s
Sweep period	0.5 ms
Spectrogram analysis window	Hamming

In time–frequency analysis, there is an inherent trade-off between time resolution and frequency resolution. When analyzing the GPS L1-C/A signals in the presence of sweep interference, the Hamming window was chosen as the window function for the spectral analysis. As shown in Figure 2b, when the analysis window length was 31 sample points, the time–frequency resolution was insufficient to distinguish the sweep interference, resulting in the interference effect being indistinct on the time–frequency plane, and the sweep interference could not be accurately detected. To improve the time–frequency resolution, the spectrogram method's time–frequency characteristics were studied by increasing the size of the analysis window. As shown in Figure 2a, when the analysis window length was increased to 63 sample points, the linear frequency modulation interference in the received GPS L1-C/A signal became more recognizable on the time–frequency plane. However, as the window length increased, the resolution in the time dimension significantly decreased, leading to suboptimal time–frequency localization characteristics. This demonstrated that while increasing the window length improved frequency resolution, it inevitably compromised time resolution. This trade-off is clearly evident in Figure 2, where it is shown that the spectrogram method struggles to provide precise instantaneous frequency estimation in practical applications. Although interference signals can be approximately assessed by appropriately selecting the window length, the spectrogram's inability to simultaneously achieve high time and frequency resolution when processing GNSS inter-

ference signals limits its application. This trade-off is common in time–frequency analysis and requires careful selection and optimization based on specific application requirements.

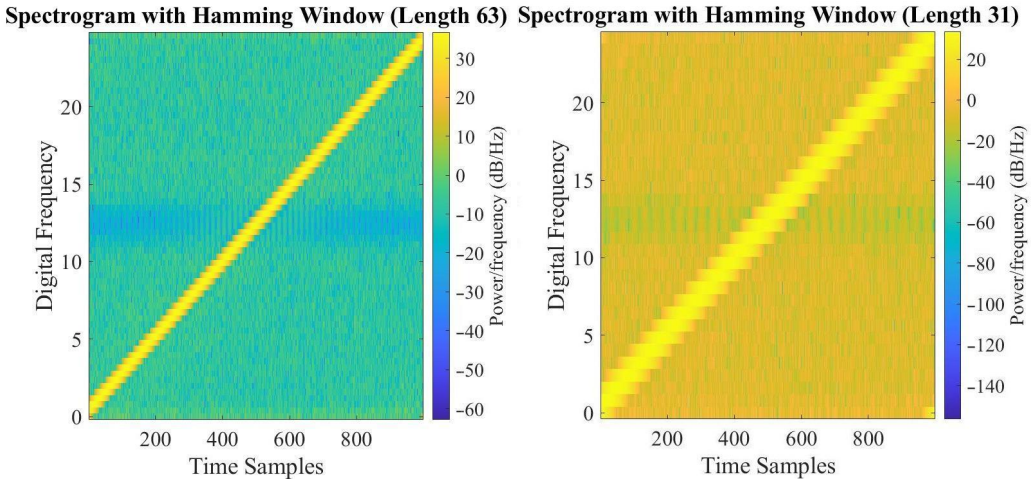


Figure 2. Using the Hamming window function for spectrogram analysis of GNSS signals: (**a**) shows the result with a Hamming window length of 63, while (**b**) shows the result with a Hamming window length of 31.

Through the analysis of this phenomenon, we have gained further insight into the limitations of time–frequency analysis tools when dealing with complex interference signals. In Figure 3, it can be seen that the LFM signal exhibited an energy concentration characteristic at the optimal fractional order. By simply applying spectral line removal at this order, the LFM interference could be filtered out, thus avoiding the issues associated with the trade-off between time and frequency resolution.

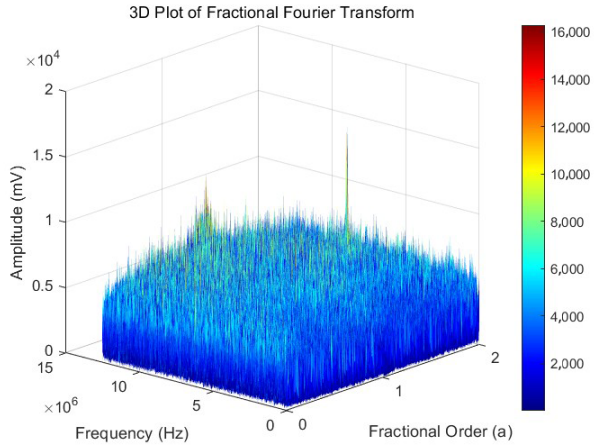
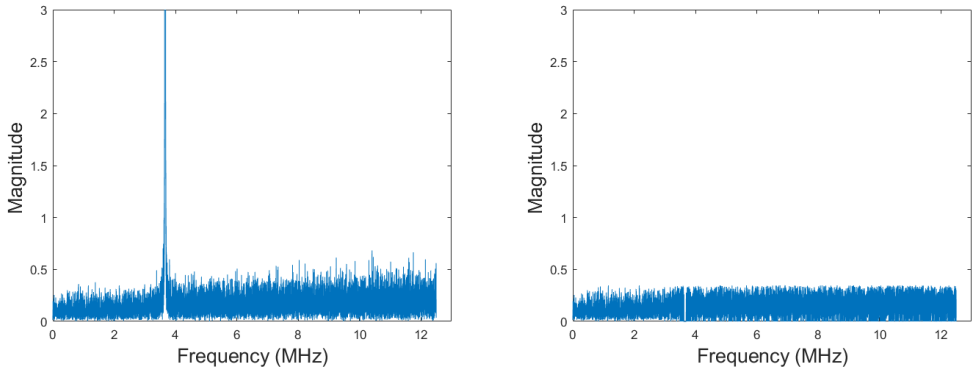


Figure 3. The 3D representation of the FrFT for the LFM signal.

The squared magnitude $|Y_p(u)|^2$ of the FrFT of the interference-affected GNSS signal is clearly depicted on the u–p plane. A distinct and sharp energy peak was observed, indicating the presence of frequency-sweep interference within the received GNSS signal. The energy peak was evidently concentrated in a very limited region on the u–p plane. In contrast, the energy contributions from known useful GNSS signals and white noise were distributed more diffusely across the u–p plane. For any fractional order of the FrFT, this portion of energy remained ineffective in accumulation and was negligible in intensity on the u–p plane.As illustrated in Figure 4a, the LFM interference signals demonstrated a significant energy concentration effect at specific fractional orders, where the signal

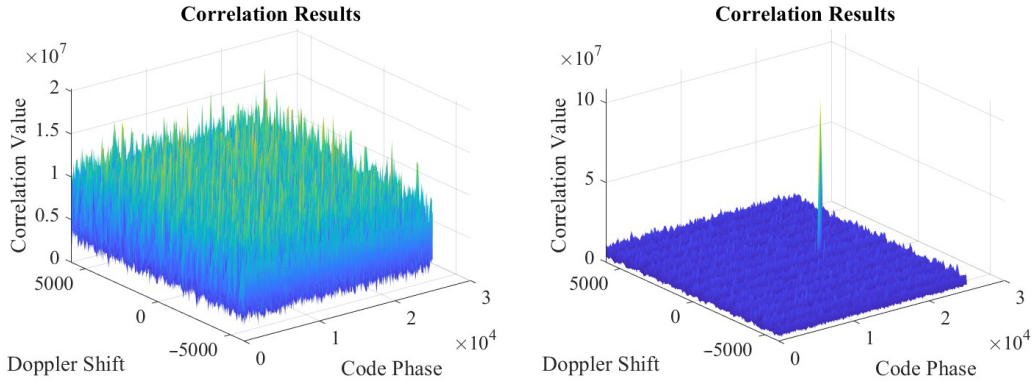
energy converged into a sharp pulse. After spectral line removal, the energy of the LFM interference signal can be significantly reduced, as shown in Figure 4b. In contrast, the GNSS signals and noise signals at the same fractional order showed a more dispersed energy distribution without a clear concentration trend. This phenomenon indicates that using the fractional Fourier transform to separate LFM interference at specific fractional orders is effective.



(**a**) (**b**)

Figure 4. Comparison of before and after spectral line removal: (**a**) before spectral line removal; (**b**) after spectral line removal.

It can be observed that, prior to filtering, the receiver was unable to capture a distinct correlation peak, as shown in Figure 5a. However, after filtering, the receiver was able to successfully capture the correlation peak, as illustrated in Figure 5b. Therefore, it is evident that this method demonstrates effective filtering performance for LFM interference.



(**a**) (**b**)

Figure 5. Comparison of the searching space before and after interference mitigation: (**a**) search result before processing; (**b**) search result after processing.

Linear frequency modulation (LFM) interference has a severe impact on GNSS receiver performance, leading to a significant degradation in positioning accuracy and, in extreme cases, a complete failure of positioning functionality. Specifically, when the energy of the LFM interference signal is relatively weak, it can prevent the receiver from reliably acquiring a sufficient number of satellite signals, resulting in inaccurate positioning solutions, as illustrated in Figure 6a. The acquisition and the tracking of satellite signals are adversely affected by the interference, leading to noticeable scattering and decreased accuracy in positioning results. When the energy of the LFM interference signal is strong, the GNSS receiver may be unable to capture valid satellite signals, thereby preventing the computation of positioning solutions, as shown in Figure 5b. Furthermore, interfering signals may increase the carrier-to-noise ratio within the channel, further impacting positioning accuracy. The interference mitigation method based on energy residual searching proposed

in this paper effectively removes LFM interference and significantly improves GNSS receiver positioning accuracy. After applying the filtering process, there was a significant improvement in positioning accuracy. Before filtering, the standard deviation of latitude was 2.5943 m, longitude was 3.1719 m, and altitude was 4.1788 m. Following the filtering, the standard deviation of latitude decreased to 0.90069 m, longitude to 1.2805 m, and altitude to 2.3074 m, indicating a substantial enhancement in the precision of the positioning data. As demonstrated in Figure 6b, after the removal of LFM interference, the positioning results from the GNSS receiver exhibited clear concentration, with substantial enhancement in positioning accuracy.

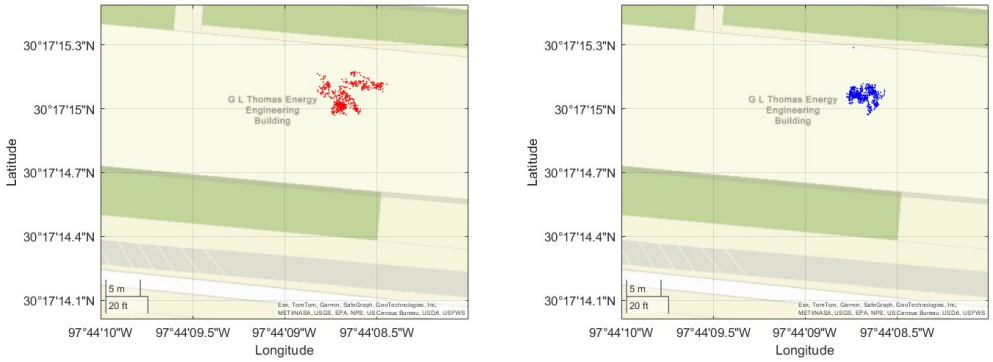


Figure 6. Comparison of positioning accuracy. The coherent integration time was 1ms, C/N0 = 40 dB-Hz, JNR = −4 dB, on the building of the University of Texas at Austin: (**a**) positioning results before processing; (**b**) positioning results after processing.

As shown in Figure 7, the experimental parameters for the Monte Carlo simulations were set as follows: the C/N_0 of the useful GPS L1-C/A signal was configured to 40 dB-Hz, the JNR value of the sweeping interference was selected as 20 dB for the CAF evaluation, the sweeping period was established at 0.5 ms, and the coherent integration time was set to 2 ms. A total of 90,000 GNSS signal acquisition tests were conducted, to obtain the detection probability and false alarm probability under various signal reception environments. We observed that the receiver exhibited excellent acquisition performance in the absence of interference. However, the presence of LFM interference significantly diminished the probability of successfully capturing the signal compared to interference-free conditions. Furthermore, it can be noted that while the application of adaptive notch filtering technology enhances acquisition performance, and the interference mitigation capability of the Wigner–Ville distribution is somewhat superior, our proposed method demonstrated improved interference resilience compared to both adaptive notch filtering and the Wigner–Ville distribution.

In Figure 8, we present the experimental parameters for the Monte Carlo simulations, where the signal's C/N_0 ranged from 35 to 45 dB·Hz, the JNR value of the sweeping interference was set to 2 dB, the sweeping period was 0.2 ms, and the coherent integration time was 1 ms. The SNR curve in Figure 8 illustrates the acquisition performance of the GNSS receiver in both interference-free and interference-affected conditions, while also comparing the effectiveness of our proposed method with the Wigner–Ville distribution and notch filtering algorithms, in terms of interference suppression. It is evident that the receiver demonstrated optimal acquisition performance in the absence of interference. However, the receiver's acquisition capability significantly declined when the received signal is subjected to interference. The use of adaptive notch filtering technology provided a gradual enhancement of the receiver's acquisition performance, albeit with limited effectiveness. In comparison, the Wigner–Ville distribution offered better mitigation of the sweeping interference; however, it remained constrained by the interference from the cross terms and failed to achieve optimal performance. Our proposed method demonstrated a

significant advantage over the previous two approaches, effectively minimizing the impact of sweeping interference to the greatest extent possible.

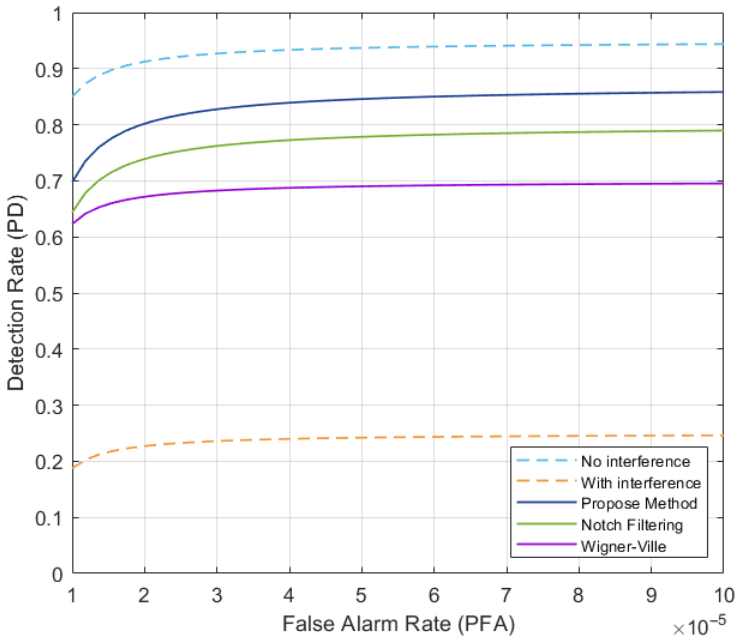


Figure 7. ROC curves of the GPS L1-C/A signal in different signal scenarios.

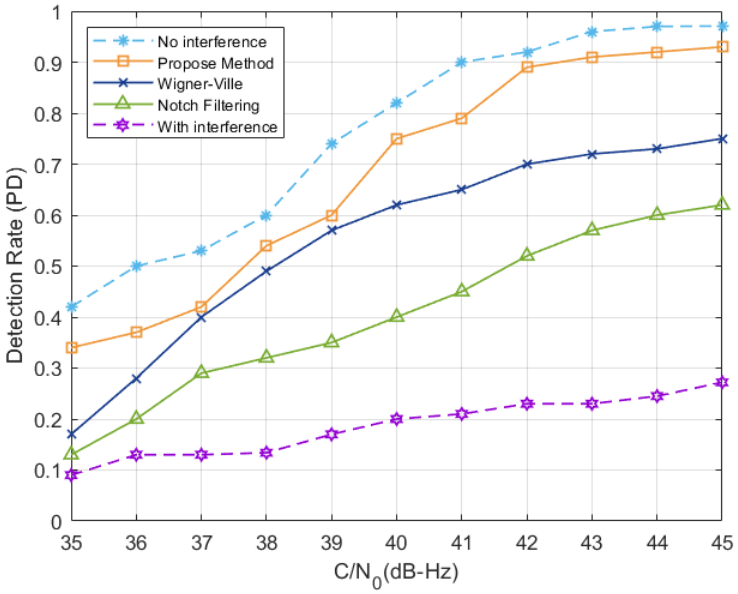


Figure 8. SNR curves of the GPS L1-C/A signal in different signal scenarios.

Furthermore, to further validate the anti-jamming performance of the proposed method, we conducted tests in real-world scenarios. Considering that the active transmission of LFM signals may involve legal issues, we simulated the interference effects by combining the interference signals emitted from a jamming device with the actual GPS L1 signal, using a signal combiner. In a converter station, electromagnetic interference is primarily manifested as high-frequency electromagnetic disturbances generated during the commutation of the converter valve on the direct-current side. These disturbances can affect surrounding equipment and measurement systems; even with shielding measures in place within the valve hall, interference signals may still propagate through wires, leading to

measurement errors. Therefore, the tests were conducted in three different interference scenarios: (1) a position 20 m from the entrance outside the DC switchyard during the converter station operation; (2) a position 500 m outside the converter station during operation; and (3) a position 2 km outside the converter station during operation. These three test scenarios exhibited varying levels of electromagnetic interference, ensuring that the method was thoroughly validated under diverse interference conditions. The capture performance of the receiver in these three scenarios is illustrated in Figure 9, which also demonstrates the interference suppression effectiveness of the proposed algorithm. The results indicate that the proposed method exhibited significant suppression of interference signals across all scenarios, further confirming its applicability in real and complex electromagnetic environments.

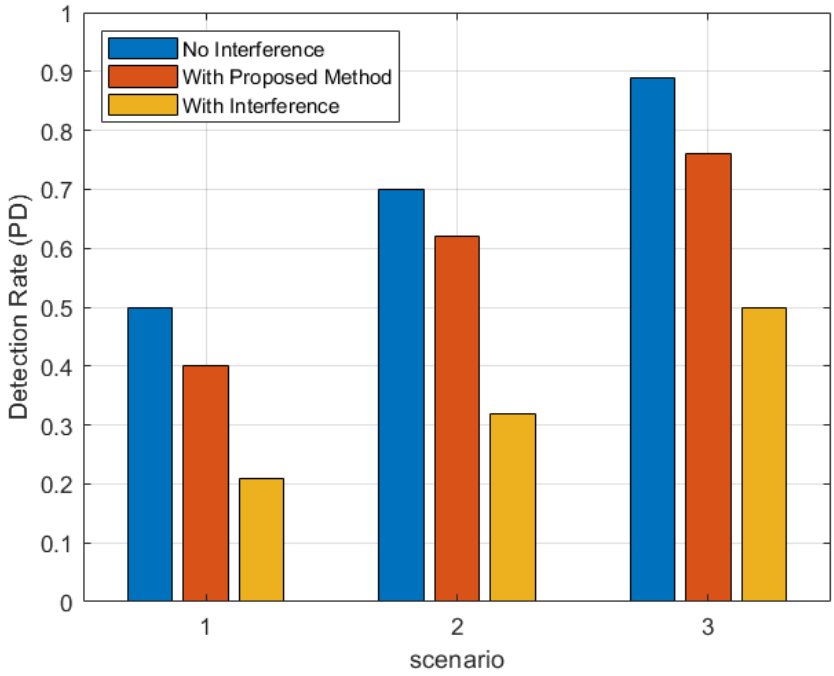


Figure 9. The interference-mitigation performance of the proposed method in different scenarios.

6. Conclusions

The overall computational complexity of our method is as follows: the FrFT has a complexity of $O(NlogN)$, the optimization process employs a variant of the Fibonacci search with a complexity of $O(logN)$, and the energy residual calculation has a linear complexity of $O(N)$. Given these complexity levels, the combined approach can be efficiently executed on platforms with moderate computational capabilities, ensuring feasibility for applications that require real-time or near-real-time processing.

This paper presents an anti-interference method based on energy residual searching to counteract the impact of LFM interference on GNSS signals. By systematically analyzing and optimizing the fractional-order parameters, the method effectively suppresses LFM interference, thereby enhancing the anti-jamming performance of GNSS signals. In our study, we first decomposed the signal, using the FrFT, which clustered LFM interference in the transform domain without significantly affecting the GNSS signals and noise. The N-sigma method calculated a threshold for the spectral component removal, eliminating high-amplitude LFM interference components. The energy residuals, defined as the difference in signal energy before and after component removal, were optimized to obtain the optimal fractional order. Our experimental results demonstrate that this approach significantly suppresses LFM interference, improving GNSS signal quality and resilience. This research offers an effective strategy for mitigating LFM interference and lays the groundwork for further studies and applications.

Author Contributions: Conceptualization, X.J.; Methodology, X.J., M.L. and Y.N.; Software, M.L. and J.W.; Validation, Y.N.; Formal analysis, J.W.; Investigation, N.X.; Resources, X.J.; Writing—original draft, Y.N.; Writing—review & editing, M.L. and N.X.; Project administration, N.X.; Funding acquisition, X.J. All authors have read and agreed to the published version of the manuscript.

Funding: This work was supported in part by the State Grid Corporation of China Headquarters Technology Project under Grant 5500-202440171A-1-1-ZN.

Data Availability Statement: The data presented in this study are openly available through TEXBAT, which can be accessed at https://radionavlab.ae.utexas.edu/texbat (accessed on 10 November 2024).

Conflicts of Interest: Author Xiaobing Jiang was employed by the company State Grid Electric Power Research Institute Co., Ltd. The remaining authors declare that the research was conducted in the absence of any commercial or financial relationships that could be construed as a potential conflict of interest.

References

1. Kaplan, E.D.; Hegarty, C. (Eds.) *Understanding GPS/GNSS: Principles and Applications*; Artech House: Mumbai, India, 2017.
2. Ioannides, R.T.; Pany, T.; Gibbons, G. Known vulnerabilities of global navigation satellite systems, status, and potential mitigation techniques. *Proc. IEEE* **2016**, *104*, 1174–1194. [CrossRef]
3. Borio, D.; O'Driscoll, C.; Fortuny, J. Jammer impact on Galileo and GPS receivers. In Proceedings of the 2013 International Conference on Localization and GNSS (ICL-GNSS), Torino, Italy, 25–27 June 2013; IEEE: Piscataway, NJ, USA, 2013.
4. Mitch, R.H.; Dougherty, R.C.; Psiaki, M.L.; Powell, S.P.; O'Hanlon, B.W.; Bhatti, J.A.; Humphreys, T.E. Signal characteristics of civil GPS jammers. In Proceedings of the 24th International Technical Meeting of the Satellite Division of the Institute of Navigation (ION GNSS 2011), Portland, OR, USA, 19–23 September 2011.
5. Kraus, T.; Bauernfeind, R.; Eissfeller, B. Survey of in-car jammers-analysis and modeling of the RF signals and IF samples (suitable for active signal cancelation). In Proceedings of the 24th International Technical Meeting of The Satellite Division of the Institute of Navigation (ION GNSS 2011), Portland, OR, USA, 19–23 September 2011.
6. Kang, C.H.; Kim, S.Y.; Park, C.G. A GNSS interference identification using an adaptive cascading IIR notch filter. *GPS Solut.* **2014**, *18*, 605–613. [CrossRef]
7. Borio, D.; Camoriano, L.; Presti, L.L. Two-pole and multi-pole notch filters: A computationally effective solution for GNSS interference detection and mitigation. *IEEE Syst. J.* **2008**, *2*, 38–47. [CrossRef]
8. Sun, K.; Jin, T.; Yang, D. A new reassigned spectrogram method in interference detection for GNSS receivers. *Sensors* **2015**, *15*, 22167–22191. [CrossRef] [PubMed]
9. Borio, D.; Camoriano, L.; Savasta, S.; Presti, L.L. Time-frequency excision for GNSS applications. *IEEE Syst. J.* **2008**, *2*, 27–37. [CrossRef]
10. Gao, G.X.; Sgammini, M.; Lu, M.; Kubo, N. Protecting GNSS receivers from jamming and interference. *Proc. IEEE* **2016**, *104*, 1327–1338. [CrossRef]
11. Konovaltsev, A.; De Lorenzo, D.S.; Hornbostel, A.; Enge, P. Mitigation of continuous and pulsed radio interference with GNSS antenna arrays. In Proceedings of the 21st International Technical Meeting of the Satellite Division of The Institute of Navigation (ION GNSS 2008), Savannah, GA, USA, 16–19 September 2008; pp. 2786–2795.
12. Sgammini, M.; Antreich, F.; Kurz, L.; Meurer, M.; Noll, T.G. Blind adaptive beamformer based on orthogonal projections for GNSS. In Proceedings of the 25th International Technical Meeting of The Satellite Division of the Institute of Navigation (ION GNSS 2012), Nashville, TN, USA, 17–21 September 2012.
13. Ouyang, X.; Amin, M.G. Short-time Fourier transform receiver for nonstationary interference excision in direct sequence spread spectrum communications. *IEEE Trans. Signal Process.* **2001**, *49*, 851–863. [CrossRef]
14. Wang, P.; Cetin, E.; Dempster, A.G.; Wang, Y.; Wu, S. GNSS interference detection using statistical analysis in the time-frequency domain. *IEEE Trans. Aerosp. Electron. Syst.* **2017**, *54*, 416–428. [CrossRef]
15. Guo, C.; Tu, W. GNSS interference signal recognition based on deep learning and fusion time-frequency features. In Proceedings of the 34th International Technical Meeting of the Satellite Division of The Institute of Navigation (ION GNSS+ 2021), Online, 20–24 September 2021.
16. Savasta, S.; Presti, L.L.; Rao, M. Interference mitigation in GNSS receivers by a time-frequency approach. *IEEE Trans. Aerosp. Electron. Syst.* **2013**, *49*, 415–438. [CrossRef]
17. Aldirmaz, S.; Durak, L. Broadband interference excision in spread spectrum communication systems based on short-time Fourier transformation. *Prog. Electromagn. Res.* **2008**, *7*, 309–320. [CrossRef]
18. Wang, P.; Cetin, E.; Dempster, A.G.; Wang, Y.; Wu, S. Time frequency and statistical inference based interference detection technique for GNSS receivers. *IEEE Trans. Aerosp. Electron. Syst.* **2017**, *53*, 2865–2876. [CrossRef]
19. Cohen, L. Time-frequency distributions-a review. *Proc. IEEE* **1989**, *77*, 941–981. [CrossRef]
20. Auger, F.; Chassande-Mottin, É. Quadratic Time-Frequency Analysis I: Cohen's Class. In *Time-Frequency Analysis: Concepts and Methods*; Wiley: New York, NY, USA, 2008; pp. 131–163.

21. Sun, K.; Zhang, M.; Yang, D. A new interference detection method based on joint hybrid time–frequency distribution for GNSS receivers. *IEEE Trans. Veh. Technol.* **2016**, *65*, 9057–9071. [CrossRef]
22. Sun, K.; Chen, Y. A novel GNSS sweep interference detection and mitigation method based on Radon–Wigner transform. *IEEE Sens. J.* **2023**, *23*, 26087–26095. [CrossRef]
23. Sun, K.; Yu, B.; Elhajj, M.; Ochieng, W.Y.; Zhang, T.; Yang, J. A novel GNSS interference detection method based on Smoothed Pseudo-Wigner–Hough transform. *Sensors* **2021**, *21*, 4306. [CrossRef] [PubMed]
24. Sun, K.; Jin, T.; Yang, D. An improved time-frequency analysis method in interference detection for GNSS receivers. *Sensors* **2015**, *15*, 9404–9426. [CrossRef] [PubMed]
25. Ashourian, M.; Sharifi-Tehrani, O. Application of semi-circle law and Wigner spiked-model in GPS jamming confronting. *Signal Image Video Process.* **2023**, *17*, 687–694. [CrossRef]
26. Sun, K.; Guo, J. A novel interference detection method based on Wigner-Hough transform for GNSS receivers. In Proceedings of the 32nd International Technical Meeting of the Satellite Division of The Institute of Navigation (ION GNSS+ 2019), Miami, FL, USA, 16–20 September 2019.
27. Almeida, L.B. The fractional Fourier transform and time-frequency representations. *IEEE Trans. Signal Process.* **1994**, *42*, 3084–3091. [CrossRef]
28. Chang, S.; Deng, Y.; Zhang, Y.; Zhao, Q.; Wang, R.; Zhang, K. An advanced scheme for range ambiguity suppression of spaceborne SAR based on blind source separation. *IEEE Trans. Geosci. Remote Sens.* **2022**, *60*, 5230112. [CrossRef]
29. Sun, K.; Yu, B.; Xu, L.; Elhajj, M.; Ochieng, W.Y. A Novel GNSS Anti-Interference Method using Fractional Fourier Transform and Notch Filtering. *IEEE Trans. Instrum. Meas.* **2024**, *73*, 8507617. [CrossRef]
30. Sun, K.; Zhang, J. Gnss interference detection test by using fractional fourier transform. In Proceedings of the 2019 IEEE 5th International Conference on Computer and Communications (ICCC), Chengdu, China, 6–9 December 2019; IEEE: Piscataway, NJ, USA, 2019; pp. 837–842.

Disclaimer/Publisher's Note: The statements, opinions and data contained in all publications are solely those of the individual author(s) and contributor(s) and not of MDPI and/or the editor(s). MDPI and/or the editor(s) disclaim responsibility for any injury to people or property resulting from any ideas, methods, instructions or products referred to in the content.